

# UNCERTAINTIES OF AN AUTOMATED OPTICAL 3D GEOMETRY MEASUREMENT, MODELING, AND ANALYSIS PROCESS FOR MISTUNED IBR REVERSE ENGINEERING

**Alex A. Kaszynski\***

Turbine Engine Division  
Air Force Research Laboratory  
Wright-Patterson AFB, Ohio 45433  
Email: Alex.Kaszynski@wpafb.af.mil

**Joseph A. Beck**

Turbine Engine Division  
Air Force Research Laboratory  
Wright-Patterson AFB, Ohio 45433  
Email: Joseph.Beck@wpafb.af.mil

**Jeffrey M. Brown**

Turbine Engine Division  
Air Force Research Laboratory  
Wright-Patterson AFB, Ohio 45433  
Email: Jeffrey.Brown@wpafb.af.mil

## ABSTRACT

*An automated reverse engineering process is developed that uses a structured light optical measurement system to collect dense point cloud geometry representations. The modeling process is automated through integration of software for point cloud processing, reverse engineering, solid model creation, grid generation, and structural solution. Process uncertainties are quantified on a calibration block and demonstrated on an academic transonic integrally bladed rotor. These uncertainties are propagated through physics-based models to assess impacts on predicted modal and mistuned forced response. Process details are discussed and recommendations made on reducing uncertainty. Reverse engineered parts averaged a deviation of 0.0002 in. (5  $\mu\text{m}$ ) which did not significantly impact low and mid-range frequency responses. High frequency modes were found to be sensitive to these uncertainties demonstrating the need for future refinement of reverse engineering processes.*


## 1 INTRODUCTION

Integrally Bladed Rotor (IBR) manufacturing deviations within standard tolerances cause dramatic rotor-to-rotor resonant response amplification [1]. This structural mistuning is a stochastic phenomenon caused by airfoil geometry variations which researchers have addressed with probabilistic approaches [2, 3]. Most published probabilistic mistuning efforts consider variations in airfoil frequency, but recent works have shown that their nominal mode shape mistuning assumptions result in forced response prediction errors on a

---

\*Address all correspondence to this author.

deterministic rotors and probabilistically predicted fleets [4,5]. Therefore, knowledge of airfoil surface geometry variations and their impact on mode shape variation is required for accurate mistuning prediction across all potential resonant ranges. Recent research has developed reduced-order models that account for geometric mistuning to enable solution times sufficient for probabilistic geometric mistuning [6–8].

A significant challenge of a probabilistic geometric mistuning approach is the quantification of airfoil surface geometry variations upon entry into service and throughout operation as parts return to depot. An automated process that collects high fidelity geometry data throughout IBR usage and then converts that data to physics-based models will enable cost effective life management. This reverse engineered physics-based model determines usability with predicted responses rather than blueprint geometry specifications. This performance-based inspection aligns with  Force Research Laboratory and NASA visions for aircraft and engine Digital Twins [9].

The reverse engineering process begins with IBR geometry measurement. Two types of geometric metrology have been used in prior research on as-manufactured airfoil response: contacting touch probe Coordinate Measurement Machines (CMM) and optical measurement systems. CMMs provide well-ordered cross section data and spot measurements, but automating such systems requires expertise in operating Computer Numerical Control (CNC) machinery. Huang et al. defined an automated system for 3D CMM measurement of turbine vane airfoils and demonstrated combined repeatability of 0.0004 *in.* (10  $\mu m$ ) [10]. While contact systems such as this are effective, the system automation requires complicated CNC system integration.

This has led to numerous examples of optical inspection systems for turbine engine components [11]. They have their own challenges when applied to IBRs: reflective surface noise, line of sight requirements, merging results from multiple scans, and unstructured data point clouds. The advantages of rapid non-contact gathering of dense spatial measurements have outweighed these challenges and encouraged continued development.

Holtzhausen et al. demonstrated a 3D optical measuring and data conditioning process for inserted-type airfoils of turbine engines [12]. The optical stereometric measurement system showed measurement repeatability within 0.0002 *in.* (5  $\mu m$ ) and approximately 30-minute scan times per blade. Lange et al. measured large populations of airfoils with this system, created steady Computational Fluid Dynamic (CFD) performance models, and showed a significant efficiency impact, particularly from leading edge variations [13]. Their work reinforced the prior discoveries of Garzon and Darmofal whose work developed similar findings, but with more conventional CMM data [14].

In the field of structural mistuning, Sinha et al. used CMM data from a commercial rotor to investigate modal variations of air-

foils [15]. Their work considered blade-alone modal response to measured deviations and used well-ordered CMM cross section measurements. Details of the method used to construct the as-measured rotor models were not provided, but the CMM data was imported into a commercial Computer Aided Design (CAD) system for solid model generation with the finite element mesh produced in commercial software. Other mistuning works with quantified airfoil geometry variation were captured with contacting probe CMM or assumed deviations for academic purposes [4, 5, 16]. These prior works have shown that small geometry variations, once considered negligible for mistuning analysis, do play an important role in response prediction, particularly for higher-order modes.

This paper contributes the use of an optical measurement system on IBRs for as-manufactured modal and mistuned response prediction. It defines a reverse engineering process that converts point cloud measurements to physics-based mistuning models. It assesses optical measurement uncertainty, and variations in the reverse engineering process, and quantifies their impact on predicted mistuned response. An automated reverse engineering process is developed to analyze repeated scans without significant user intervention. The automated process supports a maintenance depot capability to inspect and predict the response of as-manufactured IBRs. The process could be used to identify high responding rotors and remove them from the fleet prior to potential failure events.

## **2 OPTICAL SCANNING SYSTEM**

Traditional approaches for geometry measurement are based on manual or computer controlled contacting probe traces of airfoil cross sections using a measurement armature. While the process has the advantage of providing a concise set of data points, it can be very time consuming and is suited more for quality control than reverse engineering of IBRs. To address these limitations, prior efforts have attached scanning laser range-sensors to the physical armature that gather geometry measurement perpendicular to the scan path [11]. This increased the measurement resolution, but measurement time was excessive, line of sight issues prevented full scans of IBRs with closely spaced airfoils, and CNC machines with complex toolpaths were still required for automation.

Optical geometry measurement systems have seen increasing popularity associated with improvements in computer hardware data processing and high resolution digital camera sensors. Optical systems have the advantage of rapid measurement of surface data and removing the contact requirement reduces CNC process complexity. Conceptually, all sizes and types of IBR could be scanned with a series of table rotations and scanner head heights and angles. Commercial systems are available that automate the optical scanning process, but these have been focused on inserted blade measurement.

The paper demonstrates a structured light approach with a stereoscopic camera configuration for IBR measurement. The system



**FIGURE 1:** Optical 3D Scanning System

uses a central Light Emitting Diode (LED) source to illuminate the part with a regular grid pattern projection. The distorted patterns on the part are photographed by two 8 Megapixel (MP) cameras on either side of the LED source and the projected shape is used to triangulate surface coordinates. Accuracy of these systems has been shown to be within 0.0001 *in.* (2.5  $\mu\text{m}$ ) [17].

The optical measurement system used for this work is shown in Fig. 1. The scanner is elevated on the right, an advanced fan is shown illuminated by the LED in the center, and the left-hand monitor shows data captured from a single scan. Alternate camera lenses can be used to alter the size of each scan image with smaller scan patches suited to detailed parts and larger for faster digitization. A series of images are captured and merged together using common reference points created either by reflective reference circles or from annotated fixturing. Standard reference circles are used so that the measurement system automatically removes their geometry from the geometry data.

In this demonstration, the IBR was attached to a rotating CNC table allowing 360-degree automated scanning at a given scanner height and angle. After circling the part with images, the scanner head can then be manually adjusted to a new height and angle in order to capture all surfaces within the interblade passages.

Though the camera's eight MP resolution indicates the scan measurement density, in practice, only a reduced set of points within a specified depth of field are retained. The scanning software can reject measurement points within defined tolerances to further reduce the data set. With the academic transonic rotor, the maximum resolution scan contained approximately two million points. An overview of the point cloud processing is provided in the following section.

### 3 POINT CLOUD PROCESSING

A detailed assessment of commercial point cloud processing software was not conducted because the scanning system included embedded data processing software. Its capabilities include processing the cloud into a 3D mesh and comparing it to imported CAD models for quality control analysis.

Processing the 3D point clouds into an exportable mesh involves several procedures: merging, decimation, tessellation, and final editing. The merging process collects the individual scans into a unified point cloud. Techniques have been developed to minimize variation in this process and investigations show that reference markers on measurement parts simplify the process [18]. An alternative approach uses reference points on the measurement platform or fixturing instead of the part. For preliminary scans of the transonic rotor, approximately 50 reference markers were placed across the surface. The processing software identifies these markers within the point cloud, merges the scans, and removes the marker geometries from the measured part. When measuring a large rotor population, referencing the fixturing itself eliminates the time needed to sticker each IBR. The final fixturing approach used for the transonic rotor added to the rotating table a flat disk with cantilevered beams extending radially from the rim. Reference markers were placed at the beam ends and the reference disk aligned concentrically with the transonic rotor.

The merged transonic rotor point cloud contained approximately two million data points. Even with high performance computers, data processing and file storage slowed the analysis process. Many points were in low curvature areas that could be defined by fewer points (e.g. disk surface). Decimation reduces the geometry points to a tractable number for further processing. Approaches have been developed based on retaining points at measured edges and areas of high curvature [19]. The transonic rotor cloud was reduced to 500 thousand points for continue processing. Figure 2 shows a lower resolution point cloud as an example of the detail provided from the optical measurement system.

After merging, the point cloud is an unstructured IBR digitization. Tessellation generates a mesh connecting each retained data point to its three closest measurements. This process is commonly conducted through either Delaunay or Voronoi triangulation and a variety of permutations have been developed [20]. The tessellated surface can be exported to reverse engineering software for the creation of Non-uniform Rational Basis Spline (NURBS) surfaces.

Final editing is necessary when either extraneous data is captured, such as a fixture holding the scan article, or data is absent because of a geometry scanners inability to record data at highly reflective locations. Editing is conducted within software either automatically or semi-automatically and is based on local curvature computations and geometry parameterization [21]. The process of repairing point

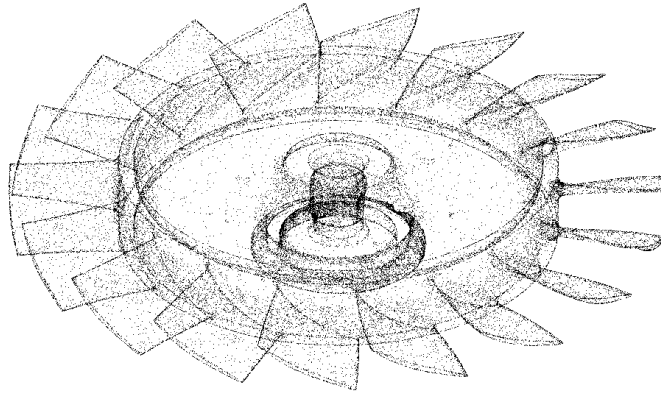


**FIGURE 2:** Transonic Rotor Point Cloud (Low Resolution)

clouds can be time consuming and, in this work, maximizing scan quality was the best approach for creating fully surfaced components. It was also found that using reverse engineering software that did not require NURBS surfacing of the entire point cloud simplified model creation.

Prior to data export, the IBR point cloud is brought into a common reference frame in a process called registration. This process conducts an optimization routine that minimizes the deviations between the scan data and a reference part. There are numerous works dedicated to improving the accuracy and speed of this process [22]. As there is no perfect solution, point cloud registration is a source of uncertainty for reverse engineered CAD models.

Several registration strategies were considered for the IBR reverse engineering process. The registration target can be the nominal CAD geometry, an averaged CAD created through reverse engineering, an existing point cloud, or the measured reference markers. Initial calculations showed merit to alignment through registration markers, but for a fleet of scanned IBRs consistent marker locations would be a challenge. To resolve this, the nominal CAD approach was pursued. It was initially assumed that the CAD provided for the transonic rotor would be sufficient as a nominal model. However, comparisons between the scan data and the CAD identified significant deviations. This is not an uncommon occurrence in practice since the pedigree of CAD models is not always known compared to the final manufactured hardware. For the transonic rotor, the scanned blade filets were approximately  $0.01\text{ in.}$  ( $254\text{ }\mu\text{m}$ ) thicker and the blade tips were  $0.01\text{ in.}$  ( $254\text{ }\mu\text{m}$ ) shorter than the nominal CAD model. A large axial shift of  $0.05\text{ in.}$  ( $1270\text{ }\mu\text{m}$ ) was found between the disk front face and the airfoil leading edges. Airfoil surfaces were within  $0.004\text{ in.}$  ( $102\text{ }\mu\text{m}$ ) of the nominal model, which was within reasonable manufacturing tolerances.

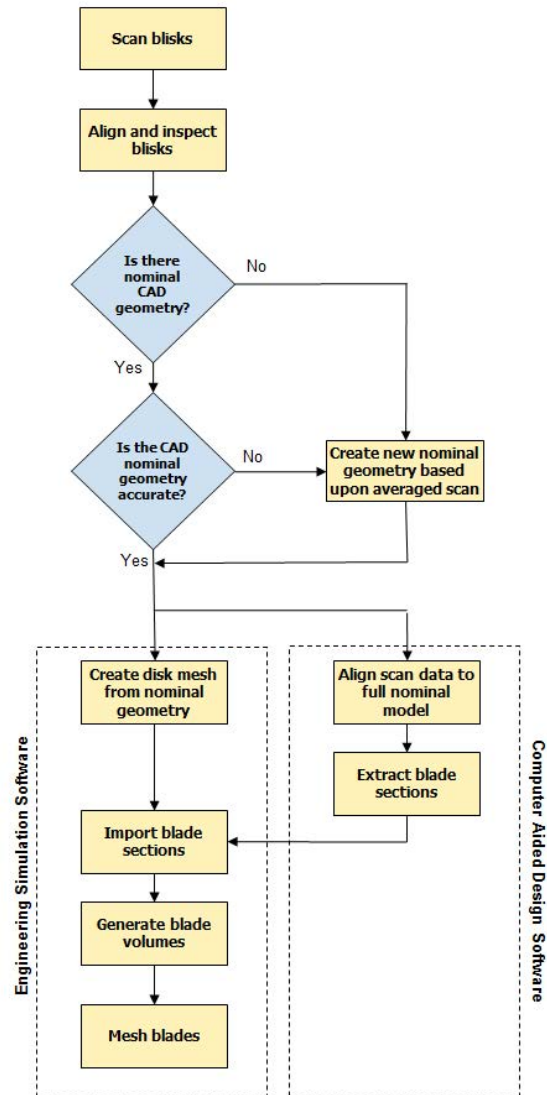


**FIGURE 3:** Automated Reverse Engineering Process

These factors made it necessary to develop an average, measured IBR CAD model based on the scan data. The inaccurate nominal model would make blisk registration less accurate, and a poorly modeled disk would reduce the analysis accuracy. This process of generating an average measured model from the first scan data set is included in the automated reverse engineering process shown in Fig. 3. The averaged IBR was created by averaging the geometries of all measured sectors.

## 4 REVERSE ENGINEERING

With a properly prepared tessellated point cloud mesh, the process continues with the reverse engineering of the data into a CAD model. Chang et al. evaluated several commercially available reverse engineering software solutions [23]. Their work concluded that the primary difference between these softwares was their emphasis on either creating NURBS surfaces or supporting solid modeling from point cloud data. For the purpose of this IBR reverse engineering effort, software that focused on solid modeling was found to be the most effective for automating the process of constructing modal and mistuning models. Generating a NURBS surface, though largely automated, required significant manual intervention to complete the process. In the developed IBR reverse engineering process, NURBS surfaces were not generated; instead, curves defining airfoil cross sections were created directly from the point cloud mesh. This minimized user intervention as airfoil cross sections could be readily extracted and the airfoil surfaces could be created by interpolation between the set.

Using the approach of interpolated cross sections, both the disk and airfoil models are made. From the first scan data set, the average disk was created from a radial cross section extracted from the data and rotated about the axis to produce an average disk sector ( $1/18^{th}$  of the IBR). Next, the tessellated airfoil data was superimposed at a common reference location and averaged to create an average geometry airfoil. Together, this disk sector and average airfoil created the new average IBR geometry for the referencing of all future transonic rotor scans.

With the defined average model, the scan data from the first measured rotor was registered so that successive scans would share a common reference frame. Once in the appropriate reference frame, the tessellated cloud disk geometry was analyzed for axisymmetry. If the disk was axisymmetric, then a single circumferential cross section could be used to create the disk surface. Analysis showed that a single cross section could be used to fit the measured disk geometry within  $0.002\text{ in.}$  ( $51\text{ }\mu\text{m}$ ). An assumption was made that this variation would not significantly impact the mistuned response. Because of this assumption, the creation of each imported transonic rotor model was simplified as only the airfoil measurements needed to be surfaced and meshed. The axisymmetric assumption is a factor that could be assessed in further detail as a source of uncertainty.

To surface the tessellated airfoil scan data, blade section lines were extracted using radial sections as shown in Fig. 4. Extracting the blade sections was not computationally intensive; a convergence study was conducted to determine the number of blade sections to extract. The root and blade tip sections remained fixed while the curves between were varied from zero to 20 while maintaining uniform spacing. The measured fillet sections began at  $0.125\text{ in.}$  ( $3175\text{ }\mu\text{m}$ ) radially above the disk. The convergence study analyzed the effect



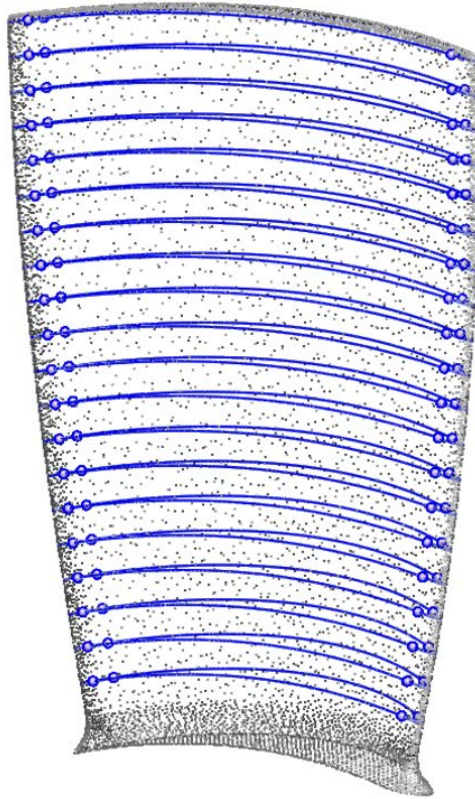


**FIGURE 4:** Extracted Airfoil Cross Sections

of blade sections on the results of a modal analysis for the modes in the frequency range.

Figure 5 shows that at eight cross sections the modal response has converged for the highest-order modes investigated in the results section. It is seen that the second chord-wise bending (2CWB) result oscillates beyond eight cross sections, introducing an uncertainty in the true modal response.

The convergence at eight cross sections is considered a relatively low number, likely driven by the low twist in the airfoil nominal design and the relatively large measured geometry deviations found and discussed later with Fig. 6. For the modes studied, the large geometric deviations outweigh smaller and more random variations. Because of this, the geometry could be approximated with the relatively low number of cross sections. More sections could be required for higher frequency modes, e.g. 3<sup>rd</sup> and 4<sup>th</sup> bend and closely spaced modes.

At this point, the disk volume has been created in the reverse engineering software and the airfoil cross sections have been extracted as curves. Geometry creation could continue within this reverse engineering software, but to ensure proper integration with the finite

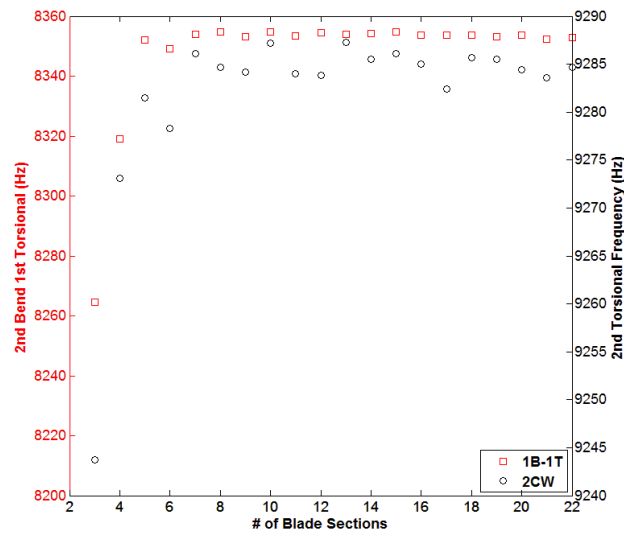


**FIGURE 5:** Airfoil Cross Section Modal Convergence

element meshing, the remaining CAD work is completed within that software.

## 5 FINITE ELEMENT MODELING

Once the reverse engineered disk and airfoil cross sections were in the finite element software, solid geometry operations were continued so that it could be meshed with hexahedral elements, a requirement to eliminate variation in sector stiffness matrices caused by variations from unstructured tetrahedral grids. These small variations are significant enough to artificially mistune the Finite Element Model (FEM) even when the geometry is cyclically symmetric.

Within the FEM software, the curves were divided into four sections (leading, suction, pressure, and trailing) at identical locations based upon a leading and trailing blade separation area. The disk volume is meshed by revolving a pattern meshed surface of quadrilateral elements. Figure 6 shows the model generation progress at this point with the mesh (blue) and the extracted curves representing each blade.

Blade volumes are generated by creating interpolated surfaces beginning from the blade/disk interface area on the nominal disk and through each curve representing one of the four surfaces of the blade. The volume generated by the four surfaces and the blade tip is then meshed by interpolating the area mesh at the root of the blade (identical at each blade for all IBRs) to the blade tip using an equal number of hexahedral elements for each blade. The base fillet surface is then projected through the disk geometry so that the hexahedral

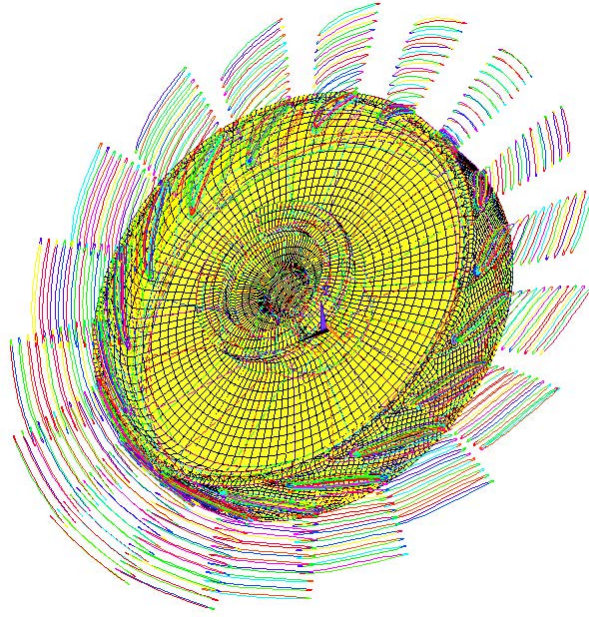


**FIGURE 6:** Airfoil Cross Section & Nominal Disk

meshing will be continuous through disk, fillet, and airfoil. This process ensures the only major variation between each FEM will be due to geometric variations between blades, and the analytical solution will not be influenced by mesh artifacts created due to mesh density variations.

The process of editing, meshing, and solving the FEM is automated through a parametric design language of the software. Since the modeling is developed through a script of analysis commands, rather than a Graphical User Interface (GUI), the final CAD modeling and finite element analysis is fully automatic once the parametric process is defined.

For a mesh convergence study, a cyclically symmetric solid model was generated from a single sector of the nominal model. Several mesh variables were assessed including the density of elements through, across, and along the span of the blade as well as modifying the density of elements on the leading and trailing edges.

## **6 RESULTS**

Prior to detailed discussion of the academic IBR, a calibration block with known dimensions and tolerances was optically scanned and reverse engineered into a CAD model. The uncertainties of this process give insight to the transonic rotor reverse engineering results.

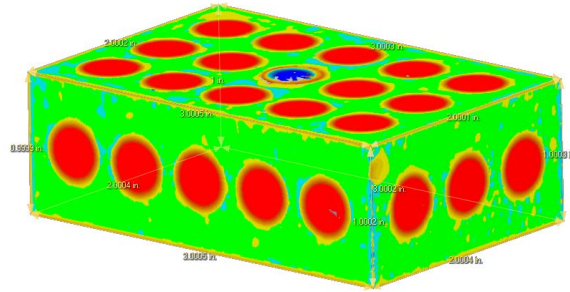


**FIGURE 7: 1-2-3 Calibration Block Scan**

## 6.1 CALIBRATION BLOCK REVERSE ENGINEERING

The 1-2-3 block is named for its 1 *in.* height, 2 *in.* width, and 3 *in.* length and Fig. 7 shows the measured dimensions and contours of deviation between scan data and CAD model. The block's series of through-holes are used for calibrating surface distances, but this was not considered in this effort. The green contours show exceedance of  $\pm 0.0002$  *in.* ( $\pm 5$   $\mu\text{m}$ ) and red indicates exceedance of  $\pm 0.0005$  *in.* ( $\pm 12$   $\mu\text{m}$ ). Each red circle shows the through-holes of the calibration block. An anti-reflective coating was not applied to the block.

The first optical scan and reverse engineered CAD dimensions showed a maximum dimension deviation of 0.0003 *in.* (7.6  $\mu\text{m}$ ) x 0.0004 *in.* (10.2  $\mu\text{m}$ ) x 0.0005 *in.* (12.7  $\mu\text{m}$ ). Given that there was visible noise in the optical scan data, five replicated scans and reverse engineered CAD models were made with an averaged model suspected to increase accuracy. The average of the five scans gave CAD dimensions 1.00017 *in.* (4.32  $\mu\text{m}$ ) x 2.00041 *in.* (10.41  $\mu\text{m}$ ) x 3.0001 *in.* (0.25  $\mu\text{m}$ ). This averaging produced a significant reduction in maximum difference between the CAD model and calibration block.

## 6.2 TRANSONIC ROTOR REVERSE ENGINEERING

Figure 8 shows the measured deviations from the average transonic IBR. Analysis of the scan data revealed that the blade-to-blade average volume variation could be as high as 8.25%. A pattern of variation can be seen from the figure by looking clockwise around the rotor starting with the thin blades (blue) to successively thicker blades (green to yellow). The significant volume variation seems to indicate either intentional or unintentional mistuning introduced through tool wear during CNC milling. If the tool wear result in thicker airfoils and the tool is replaced halfway through manufacturing, the observed pattern would be produced. These significant deviations dominate the smaller manufacturing variations and are why a small number of airfoil cross sections were needed to converge the modal

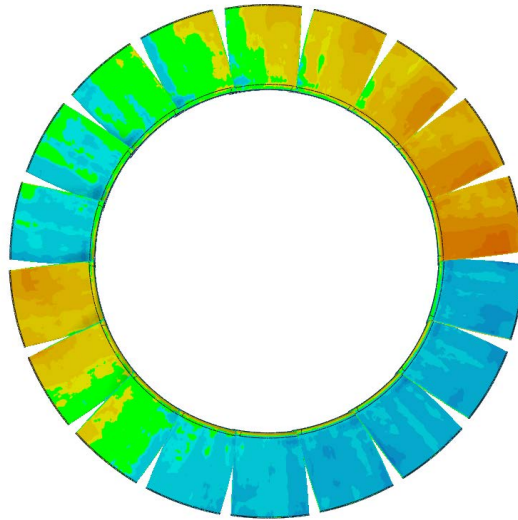


**FIGURE 8:** Measured Deviations from Average

response analysis described in [Section 4 on Reverse Engineering](#).

Figure 9 shows the average deviation from five repeated scans of the transonic rotor. The green indicates deviations less than 0.0003 *in.* ( $8\ \mu\text{m}$ ), yellow and orange are less than 0.0005 *in.* ( $12\ \mu\text{m}$ ), and the red, which can be seen only at some blade leading edge fillets, is 0.008 *in.* ( $203\ \mu\text{m}$ ) or less. Further consideration of this figure shows the largest deviations at the lower left quadrant, indicating that deviations are affected globally by the alignment process. An improved approach to align multiple scans into a common reference frame will reduce variations between scans. As is, airfoil surface deviations are below 0.0005 *in.* ( $13\ \mu\text{m}$ ). Based on prior efforts, this quantified geometric uncertainty is small enough that an assumption could be made that it would not significantly impact mistuned forced response predictions. The following paragraphs will investigate this assumption.

The impact of these deviations on the 108 predicted IBR frequencies between zero and 10,000 *Hz* is response is plotted in Fig. 10. The first 18 modes are blade localized first bending modes, the next six modes are disk dominated and show less frequency deviation, followed by the set of 18 localized first torsion blade modes. These are followed by five disk dominated modes, then 18 localized second bend models, several disk modes, localized first bend first torsion (1B-1T) mode, several more disk modes, and finally localized 2CWB.

Assessing the measurement variation on forced response, Fig. 11 shows apparent but small variations from the five replicated scans. For each frequency response function (FRF) the maximum airfoil response is plotted at each frequency. The replicated scan results are from five IBR models created from each of the scans. The average tuned response is from a cyclic symmetry model using the

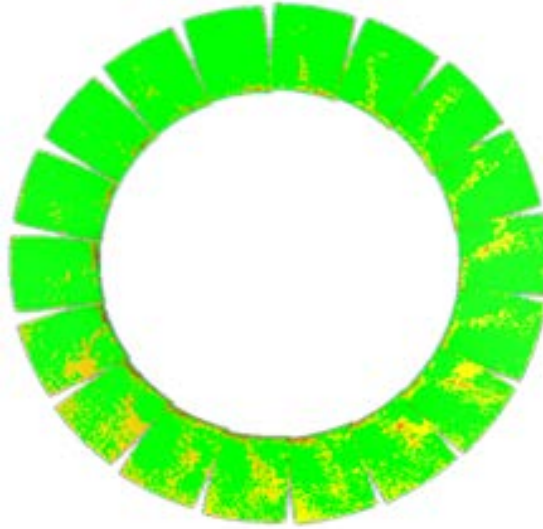


**FIGURE 9:** Average Scan-to-Scan Deviations

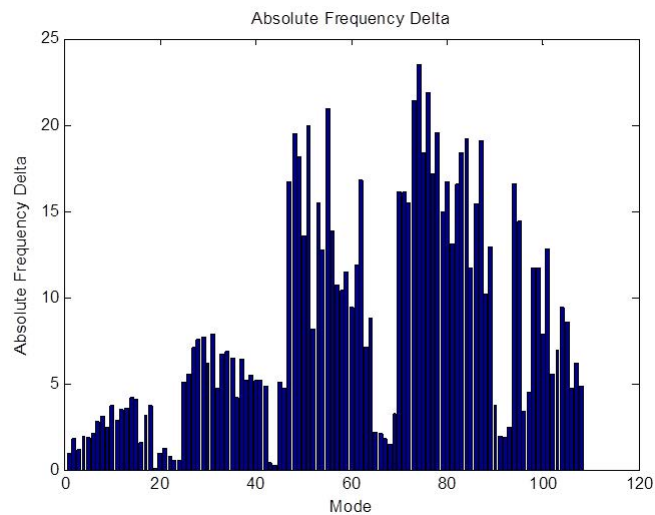


**FIGURE 10:** Absolute Scan-to-Scan Frequency Difference

averaged blade geometry calculated from the 18 measured airfoils. The mean scan mistuned response is from a mistuned rotor geometry generated from the average of the five replicated geometry measurements. The response peaks for each of the five replicated scans are tightly spaced between 1137  $Hz$  and 1138  $Hz$  and the amplitudes are between 0.1025  $in.$  (2604  $\mu m$ ) and 0.1047  $in.$  (2659  $\mu m$ ) resulting in a 2% response variation between scans.

The first torsion response of Fig. 12 shows an increased variation between replicated scans with peak response varying 0.2% between

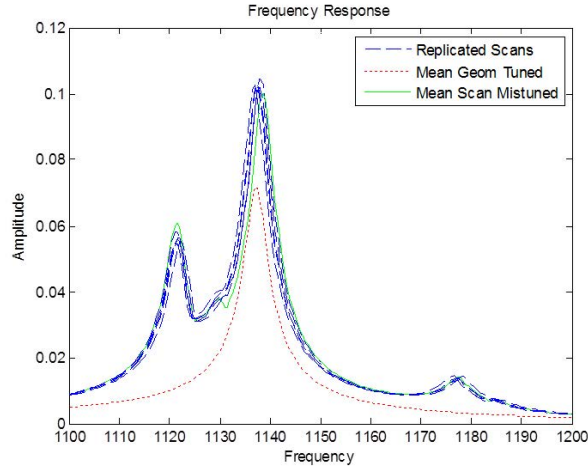


**FIGURE 11: First Bend Forced Response**

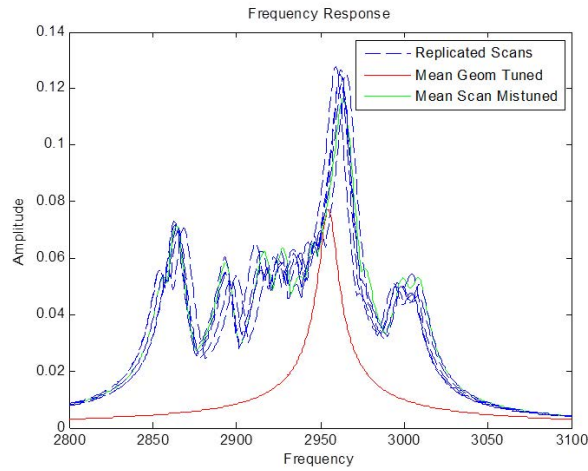


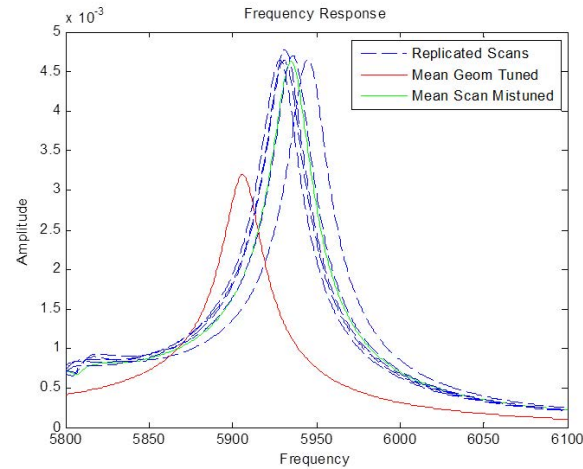
**FIGURE 12: First Torsion Forced Response**

2959  $Hz$  and 2966  $Hz$ . Its forced response ranges from 0.1222  $in.$  (3104  $\mu m$ ) and 0.128  $in.$  (3251  $\mu m$ ) for a percentage difference of 4.75%.

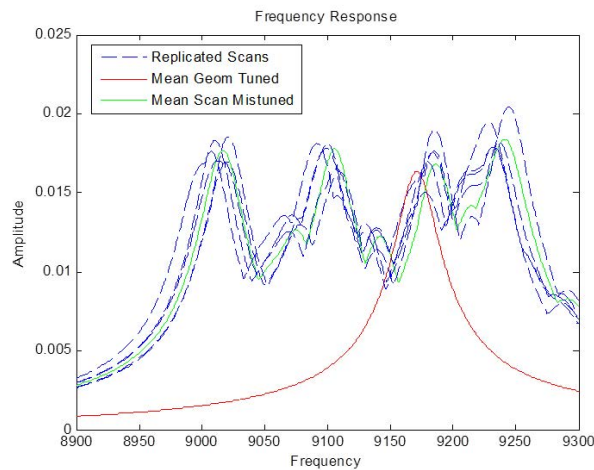
The mean replicated scan geometry for this mode showed a response below the range of the replicated scans [0.1  $in.$  (2540  $\mu m$ )], which indicates that mistunings nonlinear response does not lead to averaged geometries predicting the average of replicated scans.

Figure 13 continues to show small variations between replicated scans, even as the mode shape becomes more complex. The FRF peaks range between 5928  $Hz$  and 5946  $Hz$  for a percentage difference of 0.3% and a response variation between 4.64 E-3 and 4.78 E-3 for a 3% percentage variation. The FRF from the mean mistuned geometry, in this case, shows a response bounded by the range of





**FIGURE 13: 1B-1T Forced Response**



**FIGURE 14: 2CWB Forced Response**

replicated scans.

The final resonant condition assessed, 2CWB, is plotted in Fig. 14. The predicted frequency scatter in the peak region is still small, occurring between 9228  $Hz$  and 9245  $Hz$  (0.18% percent variation), but for this mode the variations were between 0.0179  $in.$  (455  $\mu m$ ) and 0.0205  $in.$  (521  $\mu m$ ) for a 14.5% variation. This shows that at higher frequencies mistuned response becomes very sensitive to small variations in frequency. The mean replicated scan geometry for this mode again shows that it responds within the data of the replicated scans.

Each of these result sets shows excellent repeatability between reverse engineered IBRs. And, measurement noise does not signifi-



cantly impact results. This demonstrates that this process can be used to successfully predict mistuned response.

## 7 CONCLUSION

This paper developed an IBR reverse engineering process that is sufficiently automated that a fleet of parts could be measured and analyzed. The optical scanning hardware proved a repeatable, precise ( $\pm 0.0002$  in.), and fast option for gathering geometric data. The uncertainty in the reverse engineering process was evaluated through analysis of replicated scans of a calibration block and an academic transonic rotor. For the transonic rotor, the results of the measurement uncertainty on predicted modal and mistuned forced response were calculated. Variation in predicted FRF peak amplitude resonant frequencies were each below 0.3% and for all but the 2CWB mode the response variation was below 5%. The 2CWB showed appreciable forced response variation, and indicated the need for continued investigations into reduction of the reverse engineering process uncertainty.

The repeatability of the reverse engineering method described here makes this a viable option for future depot work to verify IBR mistuned response. While this research has verified the precision of the scan to FEA process, experimental results are required in order to fully validate the accuracy of this solution. From these results, it can be determined if an optimal FRF can be obtained by averaging the geometry from multiple scans, averaging the FRFs from multiple scans, or simply scanning it once.

## REFERENCES

- [1] Castanier, M. P. and Pierre, C., "Modeling and Analysis of Mistuned Bladed Disk Vibrations: Status and Emerging Directions," *Journal of Propulsion and Power*, Vol. 22, No. 2, 2006, pp. 384–396.
- [2] Griffin, J. H. and Hoosac, T. M., "Model Development and Statistical Investigation of Turbine Blade Mistuning," *Journal of Vibration, Acoustics, Stress, and Reliability in Design*, Vol. 106, 1984, pp. 204–210.
- [3] Lee, S.-Y., Castanier, M. P., and Pierre, C., "Assessment of Probabilistic Methods for Mistuned Bladed Disk Vibration," *46th AIAA/ASME/ASCE/AHS/ASC Structures, Structural Dynamics, and Materials Conference*, Austin, TX, 18-21 April 2005.
- [4] Brown, J. M., *Reduced Order Modeling Methods for Turbomachinery Design*, Ph.D. thesis, Wright State University, Dayton, OH, 2008.
- [5] Beck, J. A., Brown, J. M., Slater, J. C., and Cross, C. J., "Probabilistic mistuning assessment using nominal and geometry based mistuning methods," *Proceedings of the ASME Turbo Expo*, Copenhagen, DEN, 2012.

- [6] Sinha, A., "Reduced-Order Model of a Bladed Rotor With Geometric Mistuning," *Journal of Turbomachinery*, Vol. 131, No. 3, 2009, pp. 031007.
- [7] Mbaye, M., Soize, C., and Ousty, J.-P., "A reduced-order model of detuned cyclic dynamical systems with geometric modifications using a basis of cyclic modes," *Journal of Engineering for Gas Turbines and Power*, Vol. 132, No. 11, 2010/11/, pp. 112502 (9 pp.).
- [8] Madden, A., Epureanu, B. I., and Filippi, S., "Reduced-Order Modeling Approach for Blisks with Large Mass, Stiffness, and Geometric Mistuning," *AIAA Journal*, Vol. 50, No. 2, 2012, pp. 366–374.
- [9] Glaessgen, E. H. and Stargel, D., "The Digital Twin Paradigm for Future NASA and U.S. Air Force Vehicles," *53rd AIAA/ASME/ASCE/AHS/AS Structures, Structural Dynamics, and Materials Conference*, 2012, pp. AIAA 2012–1818.
- [10] Huang, H., Gong, Z. M., Chen, X. Q., and Zhou, L., "SMART Robotic System for 3D Profile Turbine Vane Airfoil Repair," *International Journal of Advanced Manufacturing Technology*, Vol. 21, 2003, pp. 275–283.
- [11] Chen, F., Brown, G. M., and Song, M., "Overview of Three-Dimensional Shape Measurement Using Optical Methods," *Optical Engineering*, Vol. 39, No. 1, 2000, pp. 10–22.
- [12] Holtzhausen, S., Schreiber, S., Schone, C., Stelzer, R., Heinze, K., and Lange, A., "Highly Accurate Automated 3D Measuring and Data Conditioning for Turbine and Compressor Blades," *Proceedings of the ASME Turbo Expo*, Orlando, FL, 2009.
- [13] Lange, A., Voigt, M., Vogeler, K., Schrapp, H., Johann, E., and Gummer, V., "Impact of Manufacturing Variability and Nonaxisymmetry of High Pressure Compressor Stage Performance," *Journal of Engineering for Gas Turbines and Power*, Vol. 134, No. 3, 2012, pp. 032504.
- [14] Garzon, V. E. and Darmofal, D. L., "Impact of Geometric Variability on Axial Compressor Performance," *Journal of Turbomachinery*, Vol. 125, No. 4, 2003, pp. 692–703.
- [15] Sinha, A., Hall, B., Cassenti, B., and Hilbert, G., "Vibratory Parameters of Blades From Coordinate Measurement Machine Data," *Journal of Turbomachinery*, Vol. 130, No. 1, 2008, pp. 011013.
- [16] Brown, J. M. and Grandhi, R. V., "Probabilistic High Cycle Fatigue Assessment Process for Integrally Bladed Rotors," *Proceedings of the ASME Turbo Expo*, Reno, N.V., 2005.
- [17] Harding, K., "Latest Optical Methods for Industrial Dimensional Metrology," *Proceedings of the International Society for Optics and Photonics*, Boston, M.A., 2005.

- [18] Pauly, M., Mitra, N. J., and Guibas, L. J., "Latest Optical Methods for Industrial Dimensional Metrology," *Eurographics Symposium on Point-Based Graphics*, Zurich, SWI, 2004.
- [19] Song, H. and Feng, H.-Y., "A Progressive Point Cloud Simplification Algorithm with Preserved Sharp Edge Data," *International Journal of Advanced Manufacturing Technology*, Vol. 45, 2009, pp. 583–592.
- [20] Rindino, F. and El-Hakim, S., "Image-based 3D Modelling: A Review," *The Photogrammetric Record*, Vol. 21, 2006, pp. 269–291.
- [21] Wang, J. and Oliveira, M. M., "Filling Holes on Locally Smooth Surfaces Reconstructed from Point Clouds," *Image and Vision Computing*, Vol. 25, No. 1, 2007, pp. 103–113.
- [22] Mitra, N. J., Gelfand, N., Pottmann, H., and Guibas, L., "Registration of Point Cloud Data from a Geometric Optimization Perspective," *Proceedings of the 2004 Eurographics/ACM SIGGRAPH Symposium on Geometry Processing*, Nice, France, 2004, pp. 22–31.
- [23] Chang, K.-H. and Chen, C., "3D Shape Engineering and Design Parameterization," *Computer-Aided Design & Applications*, Vol. 8, No. 5, 2011, pp. 681–692.